Marine Chemistry 211 (2019) 25–36

Contents lists available at ScienceDirect

Marine Chemistry

journal homepage: www.elsevier.com/locate/marchem

Amorphous arsenic sulfide nanoparticles in a shallow water hydrothermal system

V.M. Durán-Toro[a,*], R.E. Price[b], M. Maas[c,d], C.-C. Brombach[e], T. Pichler[e], K. Rezwan[c,d], S.I. Bühring[a]

[a] Hydrothermal Geomicrobiology Group, MARUM Center for Marine Environmental Sciences, University of Bremen, Bremen, Germany
[b] Stony Brook University, School of Marine and Atmospheric Sciences (SoMAS), Stony Brook, NY 11794, USA
[c] Advanced Ceramics, University of Bremen, Bremen, Germany
[d] MAPEX - Center for Materials and Processes, University of Bremen, Bremen, Germany
[e] Dept. of Geochemistry and Hydrogeology, University of Bremen, Bremen, Germany

ARTICLE INFO

Keywords:
Arsenic
Nanoparticles
Hydrothermal vents
Milos

ABSTRACT

Hydrothermal fluids can contain trace elements such as arsenic (As), which are toxic to surrounding biota. In these kind of fluids, the bioavailability and biotransformation of As have been investigated but so far the ratio of total soluble As (< 200 nm) versus the amount of As contained in a nanoparticulate phase has not been reported. Here, for the first time, the presence of As in the nanoparticulate fraction (between 200 and 20 nm) is described for arsenic-rich hydrothermal fluids in a marine shallow-water hydrothermal system. Samples of diffusively venting hydrothermal fluids, pore-water and seawater were collected in the hydrothermal system located in Paleochori Bay, Milos Island (Greece), and the fraction between 200 and 20 nm ($As_{200\text{-}20}$) was studied. Up to 38% of the soluble arsenic was present within the $As_{200\text{-}20}$ fraction in pore fluids, 10 to 20% in hydrothermal fluids and 5% in seawater. Identification and characterization of particles in hydrothermal fluid, pore-water and seawater was performed by scanning electron microscopy coupled to energy dispersive X-ray spectroscopy (SEM-EDX), transmission electron microscopy (TEM) with selected area electron diffraction (SAED) and dynamic light scattering (DLS). The particles are of spherical morphology with a polydisperse size distribution (PDI: 0.37) and diameters close to 100 nm. EDX studies confirmed a chemical composition rich in As and S. The SAED pattern revealed absence of a crystal phase indicating the presence of an amorphous arsenic sulfide material. These results bring into discussion the role of the nanoparticulate fraction for As dispersion, bioavailability, and potentially harmful effects in marine coastal ecosystems.

1. Introduction

Naturally occurring nanoparticles (NPs) (i.e., sulfides, oxides or zero valent particles), can feature different physical properties compared to bulk materials (El-Sayed, 2001; El-Sayed, 2004). In the case of a marine environment these properties could significantly impact the transportation of elements within the water column, their bioavailability and potential toxicity (Boyd and Ellwood, 2010). For example, in 2011, the hydrothermal activity of deep-sea vents was established as a source of iron (Fe) sulfide NPs to the ocean (Yücel et al., 2011). The hydrothermal fluids described by Yücel et al. (2011) were rich in nanostructures of FeS_2 (nano-pyrite), a structure associated with an increased active surface area, a lower oxidation rate and a lower settling rate, when compared to macro-particles of the mineral (Yücel et al., 2011). These properties have direct implications for the biogeochemical cycling of Fe in deep-ocean ecosystems, and it was suggested as an explanation of how Fe, released due to hydrothermal activity, avoids sedimentation and thus remains longer in the water column (Boyd and Ellwood, 2010; Yücel et al., 2011).

Subsequently, research on NP fractions in hydrothermal fluids was expanded to different marine ecosystems (Gartman et al., 2014; Kadar et al., 2012; Sharma et al., 2015). Gartman et al. (2014) reported Cu and Zn pyrite-containing nano-aggregates as a widespread component in black smoker emissions from hydrothermal vents, and Kadar et al. (2012) described nano-clusters rich in Fe and Mn that aggregated into larger colloids when mixed with seawater along a pH gradient in a shallow water vent system. Thus, most of the research on NPs in hydrothermal vents to date describes the generation of metallic

* Corresponding author.
E-mail address: vduran-toro@marum.de (V.M. Durán-Toro).

https://doi.org/10.1016/j.marchem.2019.03.008
Received 19 December 2018; Received in revised form 6 March 2019; Accepted 13 March 2019
Available online 14 March 2019
0304-4203/

enrichments, forming amorphous and highly polydisperse metallic NPs, rich in Fe, Mn, Si, S or O (Kadar et al., 2012; Sharma et al., 2015). However, to the best of our knowledge, no NP fraction of potentially toxic elements such as arsenic has been investigated in hydrothermal fluids.

Arsenic is a trace element present in many hydrothermal fluids, classified as a metalloid with extremely harmful biological effects at high concentrations (Hughes, 2002; Jomova et al., 2011; Pichler et al., 2006; Price and Pichler, 2005; Price et al., 2013c). It is an element widely spread in the environment, being present in different oxidation states (typically +3 and +5 and −3), as inorganic (i.e. hydrides, AsH_3; sulfides, As_4S_4; oxides, As_2O_3) or organo-arsenic (i.e. dimethylarsenic acid, $(CH_3)_2AsOOH$ cacodylic acid, etc.) compounds (Grund et al., 2008; Price et al., 2013a). The toxicity of arsenic has been reviewed extensively and differs on a biochemical level according to its oxidation state (Hughes, 2002; Jomova et al., 2011). The two main inorganic forms of soluble arsenic are arsenate, As (V), and arsenite, As (III). Arsenate is found mainly in oxygen-rich fluids and due to chemical similarities with phosphate (PO_4^{3-}) both molecules compete by affinity for specific union sites of enzymes, resulting for example, in blocked coenzymes or substrates like adenosine tri-phosphate (ATP) (Hughes, 2002; Jomova et al., 2011). As (III) on the other hand, has a high affinity for thiol groups present in cell macromolecules (i.e., proteins), where it can alter their structure and function (Hughes, 2002; Jomova et al., 2011). The main cellular effect of As is upon cell proliferation by damaging the DNA replication and reparation system and oxidative stress by decreasing the concentration of low-molecular-weight thiols (i.e. glutathione) used in the cell redox-system (Filomeni et al., 2002; Hughes, 2002).

Arsenic is elevated relative to background seawater in many submarine hydrothermal fluids (Aiuppa et al., 2006; Breuer and Pichler, 2013; Pichler et al., 1999c; Price et al., 2013b; Price et al., 2013c), which provides an opportunity to study the cycling and particulate phases of this element in the marine environment. The shallow-water hydrothermal system in Paleochori Bay, Milos (Greece), in particular, is a natural laboratory for studying arsenic release. There, vent fluid concentrations as high as 78 μM were determined, exceeding values found in fluids of deep-sea hydrothermal systems, like mid-ocean ridge (MOR) or back-arc basins (BAB) (0.7 to 10 μM (Douville et al., 1999; Price et al., 2013c). In general, reducing hydrothermal fluids have mainly As(III), which is also the case in the Milos system, although significant concentrations of mono-, di-, and trithioarsenate were found (Price et al., 2010). In Paleochori Bay a strong hydrothermal influence is manifested by a yellow-orange (arsenic sulfide) precipitate on the sediment surface (Bühring and Sievert, 2017; Godelitsas et al., 2015), together with high temperature (> 85 °C) and low pH values (~5) (Sievert et al., 1999). Surrounding the yellow areas, white microbial mats are present at midrange temperatures (~45 to 85 °C), covering the most extensive areas of the bay characterized by sulfur and silica mineralogy (Dando et al., 2000; Dando et al., 1998; Sievert et al., 1999). In the outer rim of the hydrothermally influenced sediment, lower temperatures (~30–35 °C) and the accumulation of Fe- and Mn-oxides are manifested as brown surface structures. Arsenic sulfide precipitation in Palaeochori Bay can be explained by the high concentration of soluble sulfide (HS^-, S^{2-}) present in the fluids (~3 mM) (Godelitsas et al., 2015; Price et al., 2013c), which, together with the low pH, and reducing conditions (Price et al., 2013c) can trigger the generation of several insoluble arsenic sulfide species (Rochette et al., 2000).

Interestingly, the arsenic sulfide precipitate that accumulated on top of and within the sediments had a size 10^4 times larger than any As—S artificially produced nano-material (Table 1) (Godelitsas et al., 2015), including As_2S_3 quantum dots formed by cluster mediated transformation from orpiment bulk material or As_2S_3 nano-film generation through chemical bath deposition (Table 1) (Ubale et al., 2013; Wu et al., 2017). Among the different arsenic forms described to date, it was never found as a nano-material occurring in nature (Table 1) (Sharma et al., 2015). So far, As had been widely studied regarding its distribution as soluble species, complexation or adsorption into the particulate (> 400 nm), colloidal (< 400 nm) or truly dissolved (< 20 nm) fractions of organic matter and Fe in the water column (Bauer and Blodau, 2009; Boyd and Ellwood, 2010; Caporale et al., 2013; Guo et al., 2011; Neubauer et al., 2013; Serrano et al., 2015), without considering individual As NPs. The World Health Organization (WHO) guideline value for As in drinking water was established at 10 μg/L, although many countries operate with a limit of 50 μg/L (Smedley and Kinniburgh, 2001). In a similar way, the aquatic life ambient water quality criteria provided by the US-Environmental Protection Agency (EPA) limited the presence of As (in any oxidation state) to 69 and 36 μg/L for acute and chronic exposure, respectively, in saltwater systems. These criteria for As regulation in aqueous environments only consider soluble As (< 200 nm), and do not consider particle size variables, e.g., nanoparticles, as being part of the soluble As concentrations and with a potential different toxic impact than the "truly" dissolved species (< 20 nm) (AshaRani et al., 2009; Duran et al., 2010; Prabhu and K Poulose, 2012; Xia et al., 2008). Thus, the identification of As in a nanoparticulate fraction (200–20 nm) could be crucial for the understanding of As dispersion and bioavailability.

Milos is a promising natural model site to study arsenic in the nanoparticulate form, and provides an opportunity to understand the formation of As NPs and their potential impact on marine organisms. The present work describes, for the first time, the identification and chemical characterization of As- and S-rich NPs found in seawater, pore-water and hydrothermal fluid in Palaeochori and Spathi Bay and discusses the potential influence of As NP emissions to the coastal ocean biogeochemistry. With the present study, we want to contribute to the generation of an expanded vision of arsenic transport and toxicity, taking the unexplored but potentially significant fraction of As NP into account.

2. Materials and methods

2.1. Sample collection and determination of environmental parameters

During two sampling campaigns in June 2016 and June 2017 hydrothermal fluids (HF), pore-water (PW) and seawater (SW) samples were collected by SCUBA divers. Diffusively venting hydrothermal fluids were collected using a funnel system connected to a polyester heat resistant bag with a valve for gas release (Gomez-Saez et al., 2015). The system was placed over a venting spot in order to avoid mixing of hot hydrothermal fluids with seawater. Collection of PW samples was from a sediment depth of 10 cm using 60 mL syringes connected with a polypropylene tube to a perforated 5000 μL pipette tip (Price et al., 2013b; Price et al., 2013c). Seawater samples were collected manually by opening cleaned 1 L borosilicate glass bottles (SCHOTT) approximately 50 cm below the sea surface to ensure collection of a representative sample, avoiding major-element accumulating biofilms or other surface phenomena (Ferreira et al., 1996; Goering and Menzel, 1965; Gomez-Saez et al., 2015). HF, PW and SW samples presented in this work correspond to two specific venting sites designated in the literature as Spathi Bay (SB) and Rocky Point (RP) (Fig. 1) (Bayraktarov et al., 2013; Price et al., 2013b). One HF sample (HF1), two PW samples labeled as yellow1 (Y1) and brown1 (B1), and one SW sample (SW1) were collected from the RP area during the campaign in 2016 (see Supplementary Table 1 for a list of all samples collected). The names of PW samples were assigned based on the typical color of the sediment surface precipitates, where yellow precipitates are related to the arsenic sulfide minerals previously described in Godelitsas et al. (2015) and brown to precipitates rich in Fe and Mn oxyhydroxides (Price et al., 2013c). Y1 was the nearest sample to the venting center (~50 cm) and B1 the farthest away (~2 m). An extra SW control sample (SW2-Pollonia) was collected on the north shore of Milos from an area without hydrothermal activity (Fig. 1) (Dando et al., 1995). Additional samples

Table 1
Main As nanomaterial synthesis methods.

Method	Nanoparticle	Temperature	pH	Size/Morphology	References
Chemical vapor deposition/Thermal evaporation	$GaAs/As_2S_3$	~160 °C;	n.s.	2–6 nm/Dots; ~1,2 μm/ micro-film	(Bao et al., 2008; Choi et al., 2007; Malik et al., 2003; Soci et al., 2008; Tichá et al., 2000)
Electro-Chemical bath deposition/ SILAR	As_2S_3	6 °C; 25 °C	< 7	185–520 nm/Film 400–800 nm/Film 200–380 nm/Film	(Mane et al., 2000; Mane et al., 2004; Sartale and Lokhande, 2000; Ubale et al., 2013; Yesugade et al., 1995)
Laser ablation Laser irradiation	$GaAs/As_2S_3$	n.s.	n.s.	9–13 nm/Spheres; 30–80 nm/nano-phases; 0,1–1,4 μm/nano-lenslets	(Perrière et al., 2001; Velea et al., 2012)
Colloidal synthesis	InAs	130–240 °C	n.s.	2.5–6 nm/Dots	(Malik et al., 2005; Zhang and Zhang, 2010)
Covalent immobilization	$ZrAs\text{-}Fe_3O_4/SiO_2$	25–60 °C	n.s.	30 nm/Aggregates	(Li et al., 2012)
Chemical reduction	As^0	25–60 °C	7–9	67 nm/Spheres	(Pal et al., 2012)
Grinding	As_4S_4	25 °C	~7	50 nm/Spheres	(Wu and Ho, 2006)
Milling	As_4S_4	25 °C	~7	137–150 nm/Grains	(Baláž et al., 2009; Baláž et al., 2012; Baláž et al., 2011; Bujňáková et al., 2015; Zhao et al., 2011)
Co-precipitation	As_4S_4	40 °C	< 7	80 nm/Spheres	(An et al., 2011; Zhao et al., 2009)
Cluster-mediate transformation	As_4S_4/As_2S_3	25–140 °C	~8	3–9 nm/Dots	(Wang et al., 2008; Wu et al., 2017)
Biologically induced reduction	As_2S_3/AsS	~30 °C	~7	30–70 nm/nanotubes; 50 nm/Spheres	(Jiang et al., 2009; Lee et al., 2007; Newman et al., 1997)
Chemical reduction	Orpiment (As_2S_3)	25 °C	4–7	n.s.	(Rochette et al., 2000)*

* Precipitation of micro/macro crystals or bulk material. n.s. not specified. SILAR: Successive ionic layer adsorption and reaction.

of HF and PW were collected during the campaign in 2017 in the areas of RP (HF2) and SB (yellow2, Y2). All plastic and glass material used in the field was cleaned 3 times with 10% HCl and de-ionized water (~18 Ω, Ohm).

Temperature was measured in situ at 10 cm depth using a handheld temperature-probe in a custom-built underwater housing described previously (Sollich et al., 2017). The pH was determined using a portable pH-meter (Myron L) immediately after the samples were brought on-shore.

2.2. Sample treatment and storage

After sampling, HF, PW and SW were divided into subsamples for chemical analyses. Samples for anion analysis were filtered using

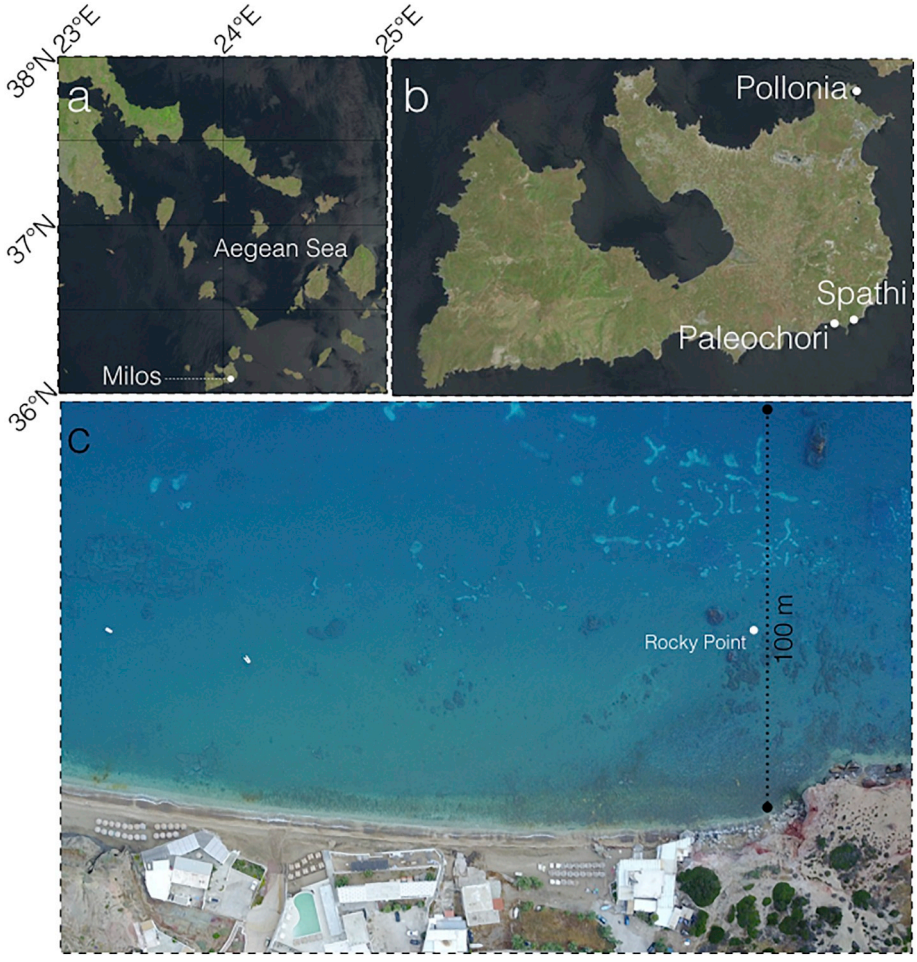

Fig. 1. (a), Regional map showing the location of Milos Island, situated in the Aegean sea in front of the cost of Athens. (b) shows the studied areas off the island. In the north, seawater samples (Pollonia, 36°45'N 24°31'E) were collected and in the south, the bays of Paleochori (36°40´N;24°30'E) and Spathi (36°40'N; 24°31'E) for hydrothermal fluids and pore-water samples collection. Images were provided by USGS GloVis, using the data set of Landsat-8. (c), drone image of the Paleochori Bay with a dashed line indicating the first 100 m of the total transect sampled, starting at 36°40'29"N and 24°30'58"E. Rocky Point area where HF1, HF2, Y1, B1 and SW1 were collected its located 50 m off shore as indicated in the figure.

0.22 μm pore size polyethersulfone (PES) filters and stored in plastic vials at 4 °C until analyses. The sample splits for cations and trace metal determination were filtered using the same type of filter, acidified with ultrapure concentrated HNO_3 to 1% acid by volume and then stored at 4 °C (Price et al., 2013c).

For NP identification and As quantification we collected at least 450 mL of sample, which then was sub-divided into 3 groups of at least 150 mL; 150 mL or more were kept unfiltered (e.g., $HF1_{uf}$, $Y1_{uf}$, $SW1_{uf}$, etc.), the remaining volume, 300 mL or more of the samples were filtered through 200 nm pore size polycarbonate filters and at least 150 mL were kept for analysis (e.g., $HF1_{200}$, $Y1_{200}$, $SW1_{200}$, etc.). Finally, the remaining sample, already filtered through a 200 nm polycarbonate pore size filter membrane was filtered through the 20 nm pore size membranes (e.g., $HF1_{20}$, $Y1_{20}$, $SW1_{20}$, etc.). Filtrations were performed using a tower filtration system connected to a vacuum pump. Each sub-group (1. unfiltered, 2. filtered through 200 nm and 3. filtered through 20 nm), was divided into 50 mL serum bottles previously flushed with N_2 and stored at 4 °C to avoid oxidation or growth of metallic sulfide particles (Yücel et al., 2011). Filters were kept at 4 °C in petri-dishes after filtration to further analyze NPs. In parallel, from each filtration process, 4 mL were collected in triplicate and acidified (1% HCl) for As quantification in the fraction between 200 and 20 nm ($As_{200\text{-}20}$).

For physical and chemical characterization, a NP extract was obtained by centrifugation of the sample in ethanol. The samples were first dialyzed overnight with a 12 KDa (< 10 nm) membrane and then diluted 1:2 with ethanol (EtOH) as described for the flocculation of metallic chalcogenide particles and other colloidal metal oxide NPs (i.e., AuO_2, ZnO, CeO_2, CdS, CdSe or CdTe) (Brust et al., 1994; Chen and Chang, 2004; Du et al., 2012; Pérez-Donoso et al., 2012; Rodríguez-Paéz et al., 2001). Finally, centrifugation was performed at 13000 *g* for 1 h at room temperature. The centrifugate was rinsed 3 times with Milli-Q water and suspended in EtOH for storage at −20 °C.

2.3. Geochemical analysis

Anion determination was performed by ion chromatography using a Metrohm IC system. A Perkin Elmer Optima 7300 DV inductively coupled plasma-optical emission spectroscopy (ICP-OES) was used for cation quantification (Pichler and Mozaffari, 2015). Samples for ICP-OES analysis were brought to a 3% HNO_3 (weight/volume; w/v) dilution to reduce problems of salinity and organic matter present in the sample.

2.4. Quantification of As

Hydride generation atomic fluorescence spectrometry (HG-AFS) was used to quantify trace concentrations of arsenic in fluid samples. The samples were prepared by adding 5 mL analytical grade 37% HCl and 0.6 mL potassium iodide/ascorbic acid solution (40% (w/v) potassium iodide, ≥ 99.5% purity) and 10% (w/v) ascorbic acid (≥ 99% purity in water) to ≤ 20 mL sample. The solution was filled up to 30 mL with de-ionized water and left standing for a reaction time of at least 30 min before quantification with the Millennium Excalibur system (PS Analytical, UK) (Pichler and Mozaffari, 2015). An aqueous solution of 0.7% (w/v) sodium borohydride in 0.4% (w/v) sodium hydroxide (Analytical grade) was mixed with the sample for the generation of arsenic hydrides from the samples and the development of hydrogen, the fuel gas for the flame. The limit of detection for the set-up was 20 ng L^{-1} As (Pichler and Mozaffari, 2015; Pichler et al., 2019; Price et al., 2007). The fraction of $As_{200\text{-}20}$ was calculated as the difference between the As concentration in As_{200} and As_{20}.

Arsenic concentrations were furthermore determined by HG-AFS for 17 samples collected along a surface and bottom transect in Paleochori Bay for the fraction As_{200} (< 200 nm). The distance between the individual samples was 20 m and thus the transect extended for approximately 320 m perpendicular to the beach (Fig. 1). Samples were collected manually by divers (~1 m below the surface and ~1 m above the seafloor) using 20 mL syringes. Each sample was analyzed in triplicate to evaluate precision. The accuracy of the measurements was verified by adding a blank and drift monitor solution after every 5 samples while using the NIST Trace 1643e and IAPSO K15 solutions as external certified references. Analytical uncertainty was determined to be better than 3%.

2.5. Electron microscopy

Unfiltered samples were analyzed by low voltage scanning electron microscopy (SEM) with energy-dispersive X-ray analysis (EDX) for NP detection and elemental analysis. After vigorous mixing, ~50 μL of sample were gently poured over carbon-stickers on top of an aluminum holder and after drying were coated with C to increase electrical conductivity required for EDX analysis. A field emission microscope (Zeiss, model iSUPRA 40) with an EDX detector (Bruker, XFlash 6|30) was operated at 4–8 kV for higher resolution imaging, while an acceleration voltage of 20 kV was used for elemental analysis (Los and Bach, 2018).

The filters used for HG-AFS quantification of $As_{200\text{-}20}$ fraction where As-NPs were detected were also analyzed by SEM-EDX. The filters were cut with scalpels, rinsed by pouring Milli-Q water on the edges of the filter to avoid detachment of NP and then dried at room temperature. Afterwards, using a plastic tweezer, the filter pieces were placed on carbon stickers for SEM-EDX analysis.

An extract of NP suspended in EtOH was obtained as described above and used to study particle morphology, crystal phase, chemical composition and size distribution by Transmission Electron Microcopy (TEM), Selected Area Electron Diffraction (SAED) and EDX coupled to TEM. The suspensions were diluted (1:10 and 1:100) and sonicated (probe sonicator) for 10 min at 40% (intensity) on ice and immediately thereafter 4 μL were dispensed on copper grids and dried overnight at room temperature. Samples were analyzed using a TEM Philips CM 20 operated at an acceleration voltage of 300 kV. Non-aggregated samples were chosen for SAED and EDX in a FEI Titan 80–300 Kv microscope.

2.6. Dynamic light scattering

Poly-dispersity index (PDI) and size distribution were studied by dynamic light scattering (DLS) using a Malvern-Zetasizer DLS system. For size distribution analyses, EtOH (HPLC grade) was used as dispersing agent and the diffraction index of the material was assumed as As_2S_3 with a value of 2.63 (Murdock et al., 2008; Rodney et al., 1958).

3. Results

3.1. Environmental parameters

Several parameters (temperature, pH, salinity, etc.) were evaluated to better understand NPs in the context of hydrothermal activity (Price et al., 2013b; Sollich et al., 2017). Table 2 summarizes the pH and temperature values of hydrothermal fluids, pore-water and seawater

Table 2
Environmental parameters for fluid samples collected during this research; Milos expedition 2016 and 2017.

Sample	Temperature (°C)	pH
HF1	83.9	5.37
HF2	96.4	5.91
Y1	99.0	4.72
Y2	65.0	5.24
B1	38.1	5.56
SW1	23.4	6.76
SW2-Pollonia	21.4	8.09

collected during the expeditions in 2016 and 2017 in Paleochori and Spathi Bay. The seawater sample collected in Paleochori Bay as a control (SW1), showed a low pH (~6.8), compared to average seawater, which indicates hydrothermal influence. For this reason, a second seawater control was taken at a location far removed from any hydrothermal activity (SW2-Pollonia) (Dando et al., 1995). The hydrothermal fluids (HF1 and HF2) had high temperatures and low pH values (Table 2). Pore-water samples (Y1, Y2 and B1), denoted a significant increase in temperature, whereas the pH remained rather constant, being close to ~ 5.4, reflecting the values of the temperature and pH of the hydrothermal fluids (HF1 and HF2, Table 2). Data indicate that the pH remains between 4 and 6 across a broad range of temperatures, from ~40 to 100 °C.

3.2. Geochemistry of hydrothermal fluids and seawater

Previous research showed that in the hydrothermal system off Milos, two distinct types of fluids discharge from the submarine vents, often within a few meters from each other: (1) a high-Cl fluid (enriched in Cl by up to 47% relative to seawater), which is depleted in Mg and SO_4 and enriched in major (Na) and trace elements (As, Br, Fe, Mn and Si), and (2) a low-Cl fluid, depleted in Cl by up to 66% relative to seawater, with additional depletions in Br, Na, Mg and SO_4 (Price et al., 2013c). As previously mentioned the RP site fluids have chemical characteristics similar to the high-Cl fluids described above (Price et al., 2013c). Thus, for samples taken from that site, we anticipated chemical compositions somewhere between the high-Cl endmember and unaltered Eastern Mediterranean seawater i.e., the control sample SW2-Pollonia. Hydrothermal fluids (HF1 and HF2) showed an increase in concentrations of Na, Cl, Si, and Mn and a decrease in SO_4 and Mg compared to SW2-Pollonia (Table 3). Pore-water samples (Y1, Y2 and B1; Table 3) also showed an influence of hydrothermal activity in their geochemical compositions, with values correlating to those found in the hydrothermal fluids (HF1 and HF2; Table 3).

There was a significant difference in the Fe content among the fluids. For example, in pore-water sample B1 (Table 3) Fe reached concentrations close to 300 µM, while in the hydrothermal fluids the element was not detected. These results correlate with data from Yücel et al., 2013 where the soluble Fe concentrations were analyzed along a transect of a venting spot and was only present in pore-water samples collected further away (> 0.5 m) from the center of the vent (Yücel et al., 2013). This is likely caused by subsurface precipitation of Fe—S and quantitative removal of Fe from the fluids (Price and Giovannelli, 2017; Yücel, 2013). Finally, other elements were variably enriched or depleted compared to SW2-Pollonia (Table 3).

An alternative way to evaluate the influence of hydrothermal activity is the amount of seawater entrainment in the samples. This common evaluation assumes that Mg is quantitatively removed at higher temperatures in the hydrothermal system, and thus any Mg in the sample is derived from seawater (prior collection). By this calculation, the sample with the least seawater entrainment is pore-water Y2, with only 12% seawater, and the one with the highest entrainment was pore-water B1, with approximately 80% (Table 3).

Table 3
Chemical composition of hydrothermal fluids (HF), pore-water (PW) and seawater (SW) samples from Milos campaign 2016 and 2017.

	HF1	HF2	Y1	Y2	B1	SW2-Pollonia
Major elements (mM)						
Cl	710.3	878.6	711.6	919.7	944.8	645.6
SO_4	20.1	8.5	26.1	6.71	13.3	32.6
Mg	39.8	25.8	24.2	6.5	41.8	52.5
Na	577.6	615.3	673.4	609.4	513.4	486.9
Trace elements (µM)						
Br	901.1	1175.1	994.9	1138.8	1197.7	964.9
Fe	b.d.	b.d.	9.5	b.d.	300.4	1.8
Mn	3.1	0.5	84.4	1.8	46.2	b.d
Si	106.3	3594.9	3484.8	2516.6	1261.7	40.9
%SW	76	49	46	12	79	100

b.d. below detection limit. %SW: Percentage of seawater present in the sample.

Table 4
Trace arsenic quantification in the nanoparticle fraction of fluids (i.e., the filtrate) from the hydrothermal system of Milos.

Sample	As_{200}	A_{20}	As_{200-20}	$\%As_{200-20}$	As_{200-20} (EM)
HF1	0.426	0.373	0.053	12.44	0.220
HF2	6.234	4.934	1.3	20.85	2.549
Y1	4.924	3.051	1.873	38.04	3.469
Y2	2.691	1.996	0.695	25.83	0.790
B1	1.312	1.151	0,161	12.27	0.767
SW1	0.094	0.089	0.005	5.32	0.005
SW2-Pollonia	b.d.	–	–	–	–

b.d. below detection limit. –: not analyzed. All the sample were analyzed in triplicates by HG-AFS. Standard deviation values ranged between ± 0.001 to 0.12. All the concentrations are given in µM scale. EM: endmember concentration.

3.3. Arsenic quantification

In order to understand the relevance of As present as a NP, total As was quantified by HG-AFS in the fraction filtered with 200 nm (As_{200}) pore-size membrane and the fraction obtained through filtration using 200 and 20 nm (As_{20}) pore-size membranes as described above. The analysis revealed the presence of arsenic in the size range between 200 and 20 nm ($\%As_{200-20}$, Table 4), starting from 5% in hydrothermally influenced seawater (SW1) to 38% in the pore-water (Y1, Table 4). The diffusively discharging hydrothermal fluids (HF1 and HF2) also contained elevated As in the same fraction, with 12 and 20%, respectively (Table 4). Furthermore, when the hydrothermal fluid endmember concentration is considered, the distribution of arsenic in the fraction between 200 and 20 nm seems to be related to seawater mixing, exhibiting a high $\%As_{200-20}$ with a high As_{200-20} endmember concentration when lower seawater mixing occurs, which suggests a dissolution effect. However, arsenic displays non-conservative behavior in the water column, being influenced by phenomena like coprecipitation with Fe oxide particles which should be considered (Pichler et al., 1999c).

In order to comprehend the influence of overall As fluxes and transport in the bay the distribution of As in the seawater along the venting area was evaluated. Fig. 2, shows two transects of soluble arsenic transport within Paleochori Bay (at the surface and close to the bottom). Both transects show clear maxima close to the venting area, with values around 7 and 3 µg/L in the bottom and in the surface, respectively. Those values decrease with distance from the area of hydrothermal activity, until reaching a value around 1.5 µg/L, which is considered the average concentration for seawater (Smedley and Kinniburgh, 2001).

3.4. Nanoparticle identification

As a first approach, SEM-EDX analysis of unfiltered samples allows a general overview of the particle diversity. Unfiltered samples of hydrothermal fluid ($HF2_{un}$) and pore-water ($Y1_{un}$ and $Y2_{un}$) showed a uniform presence of aggregated spherical particles with diameters ranging from 50 to 200 nm (Fig. 3). Despite the difference in location and sampling time, all particles had a similar morphology (Fig. 3a–c). In all areas of the samples, EDX spectra showed similar elemental compositions, indicating NPs rich in As and S with minor presence of Cl and K (Fig. 3d). To the best of our knowledge, this is the first description of naturally occurring As-rich NP associated with marine hydrothermal activity.

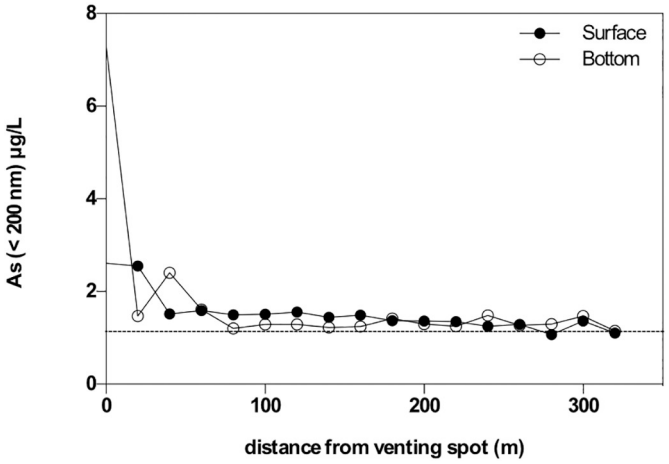

Fig. 2. Arsenic quantification in a transect along the bay of Paleochori during expedition Milos 2016. Samples of seawater were obtained in two parallel transect, in the surface (black circles) and close to the bottom (white circles). Samples were collected every 20 m approximately starting on top of a the venting spot close to the shore extending from 36°40′29″N, 24°30′58″E to 36°40′7″N, 24°30′58″E. The dashed line marks the average concentration of the last sample collected in the transect an is used as a background value of the area.

In the hydrothermal sample $HF1_{un}$ micro- to macro-particles (µm to mm scale) with highly irregular structures were found (Supplementary Fig. 1, SF1a–b). The EDX spectra showed peaks for Fe, S and Si (SF1c) indicating the presence of FeS or FeS_2 with some enrichment in silica as suggested in the literature (Gartman et al., 2014; Yücel et al., 2011). Nevertheless, no nano-structures associated with As were observed. Sample HF1 was collected in a spot with abundant streams of gas bubbles where FeS or FeS_2 precipitation took place. Indeed, precipitation of Fe sulfides from hydrothermal gas was observed in other, similar shallow-water hydrothermal systems (Pichler et al., 1999a). This may explain the absence of NPs in this sample, as it is not a true fluid sample like $HF2_{un}$, but a mixture of hydrothermal gas and seawater.

Pore-water $B1_{un}$ had a uniform particle population with a grain-aggregated morphology and particle sizes above 200 nm (Supplementary Fig. 2, SF2a–b). These aggregates were enriched in Fe, Si and O, which correlated well with the elemental composition of the fluids (SF2c and Table 3, respectively) and with the precipitation of silica-rich Fe oxyhydroxides described for other shallow Fe rich hydrothermal systems (Pichler and Veizer, 1999). However, no As was present in the EDX spectra and no other NP structures were identified. The rest of the unfiltered samples showed no representative abundances of defined particles or structures. Although seawater (SW1) could have been influenced due to mixing with hydrothermal fluids, no As, S, Fe, or Si NPs were found (data not shown).

Even though the analysis of unfiltered samples allows an overview of NP presence, the precipitation by simple evaporation (see material and methods section) of the different compounds present in the sample could alter the amount, morphology, size or elemental composition of the particles. In order to distinguish natural NP from possible artifacts, filters used for $As_{200–20}$ quantification in sample HF2 were also analyzed by SEM-EDX. Fig. 4 shows the presence of different sized nanospheres trapped on the 200 and 20 nm pore size membrane filters (Fig. 4a-b). The presence of the particles on both filters confirms the existence of an As-rich NP fraction in the hydrothermal fluids. Fig. 4c summarizes the elements atomic weight percentage (At.%) obtained from the EDX analysis where the spectrum showed only As, S and O peaks. When compared to an orpiment powder standard the sample had a slightly different As/S ratio (0.66; Fig. 4c), which was most likely due

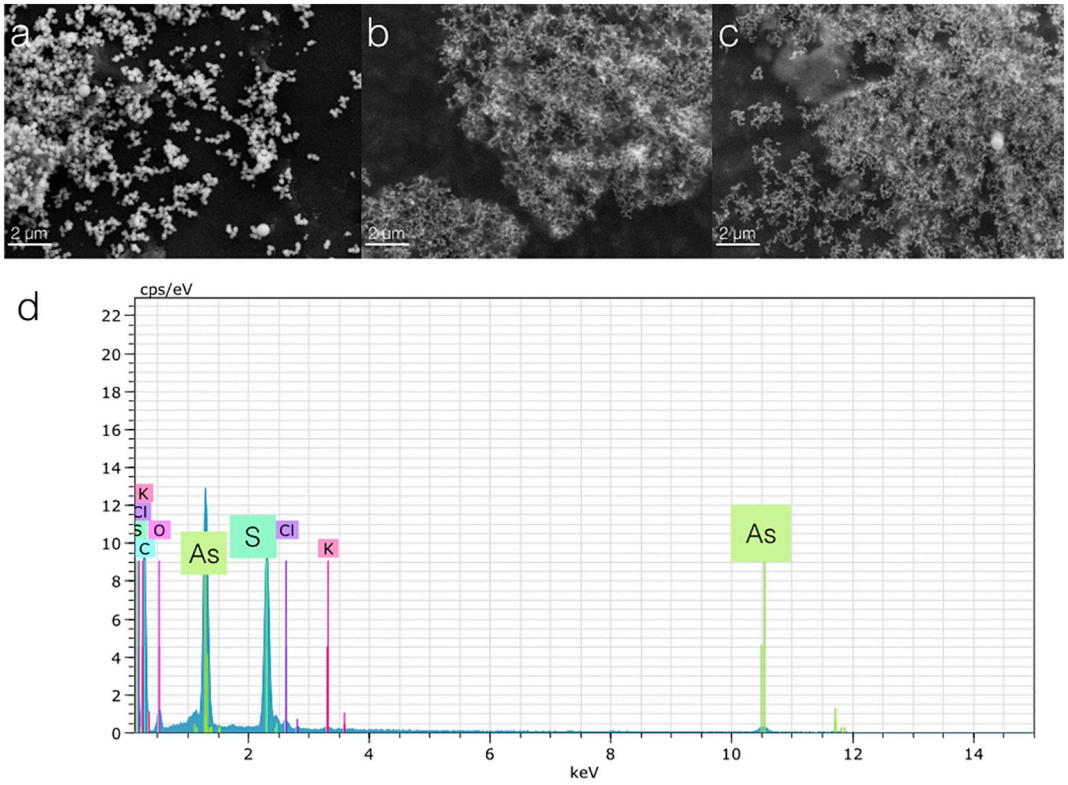

Fig. 3. SEM-EDX analysis of As–S NP from unfiltered samples of hydrothermal fluids and pore-water samples. Spherical nanoparticles with a size between 50 and 200 nm were found in hydrothermal fluids HF2 (a), pore-water samples Y1 (b) and Y2 (c). (d) EDX spectrum of particles from hydrothermal fluid HF2, enriched mainly in As, and S, with minor contributions of other elements like Cl and K. EDX analysis was repeated in different zones of the sample and in all the areas sampled, showing similar results (data not shown).

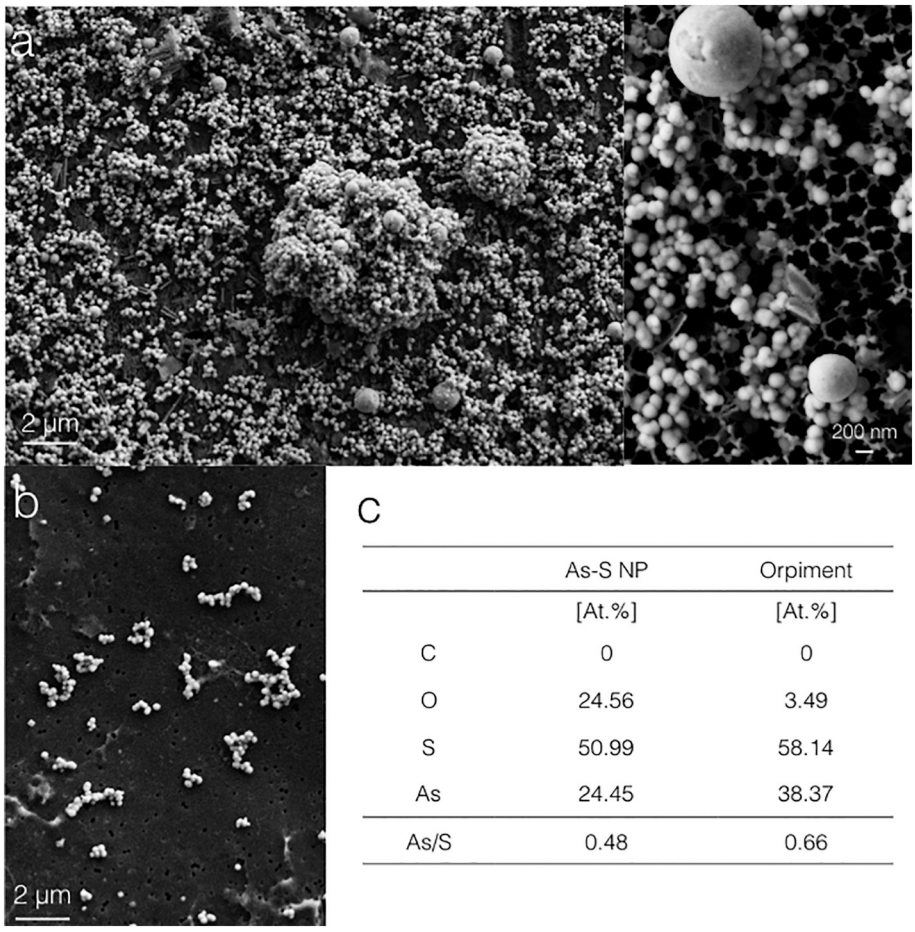

C

	As-S NP	Orpiment
	[At.%]	[At.%]
C	0	0
O	24.56	3.49
S	50.99	58.14
As	24.45	38.37
As/S	0.48	0.66

Fig. 4. SEM-EDX analysis of As—S NP collected by filtration of hydrothermal fluids from the shallow hydrothermal system off Milos. Images of the nanoparticles present in HF2 trapped on a filter of (a) 200 nm pore size are shown in two different magnifications (left and right), and of (b) 20 nm pore size. (c) Table with the atomic weight percentage (At.%) from EDX spectra of sample HF2 showing an As/S ratio between values of each element. Orpiment values were obtained from a fresh orpiment powder used as standard. At.% were normalized according to C content.

to a higher oxygen and a lower arsenic and sulfur content in the sample. This suggests the presence of oxidized forms of As or S (arsenic trioxide, arsenic pentoxide, sulfate etc.) as part of an arsenic-sulfur material potentially different from orpiment.

3.5. Nanoparticle characterization

Based on the results of the NP identification, a concentrated fraction of NPs from the sample $HF2_{un}$ was obtained by EtOH precipitation as described in materials and methods. TEM analyses showed a detailed image of the spherical structures described previously with diameters ranging between 100 and 150 nm (Fig. 5a). Typically, amorphous materials present a ring pattern during electron diffraction, which was observed (Fig. 5b) indicating the absence of a crystalline structure. The same area was analyzed by EDX confirming that the amorphous NP consists of mainly As and S, while at the same time discarding the presence of crystalline orpiment (Fig. 5c). Finally, DLS experiments determined a PDI value of 0.37, which implies a polydisperse size distribution of the particles with a peak size close to 100 nm and an average diameter size of 245 nm (Fig. 5d), which was in accordance with the microscopic analyses (Fig. 4 and 5a).

4. Discussion

4.1. Formation of As—S NP under hydrothermal conditions

The shallow-water hydrothermal system in Paleochori Bay presents remarkable environmental characteristics that lead to the formation of As—S NPs. Fluids enriched in As(III) and sulfide (S^{2-}, HS^-) are probably the significant drivers of this phenomenon (Price et al., 2013c). It was suggested that As and sulfide form As(III) sulfide species (Godelitsas et al., 2015), which precipitate on the seafloor as poorly-crystalline arsenic sulfide when the hydrothermal fluids mix with oxygenated seawater (Godelitsas et al., 2015; Price et al., 2013c). Among those several As(III) sulfide species, di- and tri-thioarsenite monomers, dimeric or trimeric arsenic sulfur and orpiment can result from a fundamental ratio between As and S present in solution at pH values around 4–6 (Rochette et al., 2000). Furthermore, a study of solubility of amorphous As_2S_3 in the temperature range from 25 to 90 °C found that the decrease in temperature and pH are the dominant mechanisms for the precipitation of amorphous As_2S_3 in hot spring systems (Eary, 1992). Hence, in Paleochori Bay the increase in pH as a result of seawater mixing with hydrothermal fluid is not considered as the main driving mechanism of formation, rather the reduction in temperature could be the key parameter inducing the precipitation of As—S NPs. It is important to note that hydrothermal fluids HF2 and pore water samples (Y1 and Y2), in which the NPs were detected, presented a yellow coloration at the moment of filtration, which indicates the presence of As—S rich material. The filtration took place immediately after samples were brought to on-shore facilities. A sampling or storage effect, by reducing the temperature of the sample cannot be completely excluded. But since results were reproducible with unfiltered samples, even after a week of fieldwork, without showing aggregation or bigger particle size due to storage at low temperature (4 °C), we assume an insignificant influence from sampling and storage. Therefore, the NPs characterized from the HF2, Y1 or Y2, are very likely to be occurring at the sediment-water interface as diffusively venting fluids mix with seawater (%SW, Table 3).

There is a significant body of literature about temperature relevance in NPs synthesis. Kinetic studies in NP generation highlight the importance of temperature in controlling the size during events of nucleation and growth (Gersten, 2005; Masala and Seshadri, 2004;

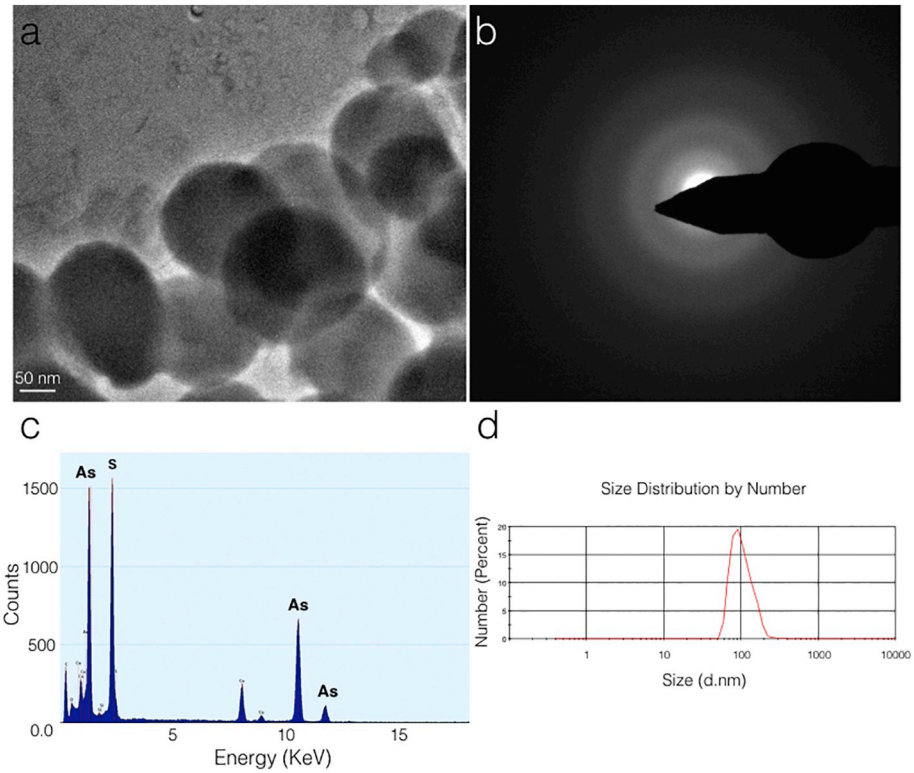

Fig. 5. Characterization of As—S NP present in hydrothermal fluids from the shallow hydrothermal system of Milos. (a) HR-TEM image of the nanoparticles precipitated by centrifugation from sample HF2 in ETOH (1:2). (b) Selected area electron diffraction of NPs from sample HF2. The patron shows no crystal phase associated to the selected area of analysis. (c) EDX spectrum of the selected area showing peaks only for As and S. The Cu signal represent artifacts from the grid used during the analysis. (d) DLS analysis of nanoparticle suspension in ETOH showing a peak size of 91 d.nm, an average size of 245 d.nm. and a PDI of 0.37.

Rajamathi and Seshadri, 2003). In the case of chalcogenide materials, which consist of a metal or metalloid (e.g., As) and an element from group 16 of the periodic table (e.g., S, Se, Te, etc.), the synthesis of NPs can be achieved by solvothermal methods that constitute hydrothermal conditions similar to those present in Paleochori Bay (aqueous solvent, 30–90 °C, pH 4–6 etc.) (Gersten, 2005; Masala and Seshadri, 2004; Rajamathi and Seshadri, 2003). Solvothermal synthesis corresponds to solution-based reactions carried out near the boiling point of the solvent, to prepare thermodynamically stable and metastable species that will take part in the formation of a new solid phase (nanoparticles) through nucleation events (Gersten, 2005; Rajamathi and Seshadri, 2003). The nucleation mechanisms of NPs have been discussed in depth in literature since they represent a key step in controlling size, morphology, and properties and its direct link to the temperature of the system (De Yoreo et al., 2015; Thanh et al., 2014; Van Hoang and Ganguli, 2012). The nucleation rate of a nanoparticle, strictly depends on the temperature control over supersaturation of the species in solution (Thanh et al., 2014). Since most of the arsenic sulfide species have a low solubility at 25 °C (Eary, 1992), a continuous temperature decrease of the initial As and S rich end-member fluid (> 90 °C) by diffusive discharge along the sediments will favor supersaturation of arsenic sulfide species and increase nucleation rate, enhancing the generation of a new phase that precipitates as amorphous nanoparticles. This also explains the lack of As—S NPs in samples with low As concentrations (HF1 and B1, Table 4), probably not reaching supersaturation conditions or nucleation rates high enough to sustain the formation of the particles. A simple way to determine saturation indices of arsenic sulfide species in the different samples is the use of "geochemical reaction models". Yet, arsenic sulfur species (e.g., As_2S_3, mono-, di-, thioarsenate or thioarsenite) present in the NPs remain unclear. The SAED analysis of the particles (Fig. 5b) indicates an amorphous material and the EDX spectrum (Fig. 4c) shows a ratio of As:S differing from As_2S_3. This suggests that a pure precipitation of orpiment or amorphous As_2S_3 during NPs formation is unlikely, but rather a participation of more than one arsenic sulfide species might occur. On the other hand, nucleation mechanisms are not considered under equilibrium condition of simple geochemical models, and even more, the nucleation of amorphous nanoparticles is poorly understood and normally crystalline nucleation models are assumed (Thanh et al., 2014; Van Hoang and Ganguli, 2012). The work of Jun et al., 2016 represent a tremendous effort to understand in situ and real-time effects on water chemistry and substrate identity on nanoscale precipitates. They used simultaneous small-angle and grazing incidence small-angle X-ray scattering (SAXS/GISAXS) to study interfacial energies between nuclei and surfaces during Fe and $CaCO_3$ nanoparticles formation, which if coupled to X-ray absorption near edge structure (XANES) can also be used to determine arsenic sulfur species present in the NP and the thermodynamic parameters of nucleation. This could be perused in future experiments to generate geochemical models of nanoparticle precipitation under hydrothermal conditions.

4.2. *Importance of nanoparticles for As cycling in the coastal ocean*

Our study reveals the presence of an important percentage of As in the nanoparticulate fraction (200–20 nm, Table 4) in hydrothermal fluids and pore-water samples, which raises the question of how surrounding biota interact with this phenomenon. For As—S NP, to the best of our knowledge, no studies on their biological effect in a natural marine environment have been performed, but investigations on cancer cells showed their enhanced bioavailability causing programmed cellular death (apoptosis) and anti-migration (metastasis) effects (An et al., 2011; Baláž et al., 2009; Baláž et al., 2012; 2011; Bujňáková et al., 2015; Wu and Ho, 2006; Zhao et al., 2009, 2011). Changes in bioavailability due to particle size can have direct toxic implications for the inhabiting organisms of a marine ecosystem. As mentioned before, metallic and metalloid sulfide materials have low solubility in aqueous solutions (pH 4–6, 25 °C) and aggregation of colloidal material can occur. Therefore, a vast majority of the arsenic sulfide particles, including the amorphous As—S NPs may (1) destabilized and dissolve, and/or (2) sink to the seafloor surrounding the venting area. The first scenario implies a direct relation between stability of particles and pH, which has been described for amorphous As_2S_3 with increased

solubility at pH 6–8 (Eary, 1992). Arsenous acid (H_3AsO_3) is the dominating species in acidic (pH ~ 4) sulfide-deficient solutions, and when an excess of sulfide is present, $H_2As_3S_6^-$ is the main soluble species (Eary, 1992). The dissolution and oxidation of amorphous arsenic sulfide were also studied by others (Floroiu et al., 2004; Lengke and Tempel, 2001). During dissolution experiments at pH 5 to 8 with or without O_2, S species can vary from $H_2S_{(g)}$ (pH 5, no O_2), to elemental sulfur and polysulfides (S_n^{2-}), to being the most common formation pathway of polythionates (S_nO_6; pH 6–8) (Floroiu et al., 2004; Lengke and Tempel, 2001). On the other hand, As(III) can account for the 96% of arsenic species dissolved (pH < 6) to 76% (pH 8) when no O_2 was present, while in O_2 rich solutions at pH 8 the percentage can decrease to a value of below 50% (Floroiu et al., 2004; Lengke and Tempel, 2001). Hence, NPs either in the water column or in the pore-water are being destabilized by an increase in pH and along a decreasing gradient of soluble sulfide concentrations as it occurs in Paleochori Bay (Fru et al., 2018; Price et al., 2010; Price et al., 2013c; Yücel, 2013). This correlates with the distribution of arsenic resistance genes in microbial communities in pore-water around venting areas of Paleochori bay as described by Fru et al. (2018). The study of As(III) oxidase (*aoxB*) and As(III) membrane extrusion (*acr3-1*, *acr 3-2* and *arsB*) genes along a gradient of soluble sulfide, showed a decrease in abundance of arsenic resistance genes when a higher concentration of sulfide was present in the pore-water, suggesting a sequestration of As(III) in sulfide minerals and therefore a lower interaction with the microbial community due to reduced mobility (Fru et al., 2018). A similar phenomenon could explain the stability of the amorphous As—S NPs, the closer they remain to the venting spot, the more stable the conditions are (pH < 6, high [S^{2-}, HS^-]), avoiding dissolution and oxidation and therefore decreasing their toxicity.

On the other hand, various microorganisms exists that are able to gain energy for growth from arsenic (e.g., arsenotrophy) (Akerman et al., 2011; Meyer-Dombard et al., 2012; Price et al., 2007). The three main types of arsenotrophs far known to occur are heterotrophic arsenite oxidizers, chemotrophic arsenite oxidizers, and dissimilatory arsenate-reducing prokaryotes (Oremland and Stolz, 2003). Price et al. (2013b) evaluated prokaryotic diversity at Milos by comparative analysis of 16S rRNA clone sequences and *aio*A-like (arsenic oxidation) functional genes (AFGs). The results indicated AFGs affiliated with either Alpha- or Betaproteobacteria distantly related to described representatives. Most clones (89%) were originated from a deeper layer of low salinity and high soluble arsenic concentrations, which overlap with the 16S rRNA data, suggesting arsenotrophy as a metabolism present in Milos that operates best at low salinity, and under anoxic, dark, sulfide and arsenic-rich conditions. However, the metagenomic analysis of the microbial community associated to an As(III) and As(V) gradient in Milos (Fru et al., 2018) indicated the predominance of genes regulating up-take and extrusion of As(III)/(V) over genes related with the use of As as an electron donor/acceptor, suggesting a low probability for the amorphous As—S NP to be used as a source of energy during arsenotrophic metabolism.

Another possibility is the use of the As—S NP to sustain sulfur-oxidizing metabolisms. In Milos, the white mats are dominated by sulfur-oxidizing *Campylobacteria* (formerly Epsilonproteobacteria) (Bühring and Sievert, 2017; Giovannelli et al., 2013; Price et al., 2013b), which use soluble sulfide present in the fluids to generate energy for their autotrophic life style. These dissolved sulfide oxidizing microorganisms might get competition by mineral-sulfide oxidizing chemolithoautotrophs using the As—S NP in the upper (sulfide deficient) sediment layers of the hydrothermal sediments of Milos, where soluble sulfide content is low due to reactions with oxidized seawater. A comparable phenomenon has been shown for sulfide deposits of ceased hydrothermal deep-sea systems, were levels of soluble sulfide are decreased, and where metaproteomic data identified autotrophic sulfide-oxidizing Gammaproteobacteria potentially facilitating metal-sulfide dissolution from sulfide deposits via extracellular electron transfer (Meier et al., 2019).

Minerals may also play a role in the stability, and thus distribution, of the As NP fraction. Iron sulfides and oxy-hydroxides are both minerals known to occur in hydrothermal plumes and play an important role for As adsorption and transport, controlling the arsenic concentration in solution (Couture et al., 2013; Pichler et al., 1999a; Pichler et al., 1999c). In the case of hydrothermal fluid HF1 (SF1) and pore-water B1 (SF2), no As NPs were found, but instead Fe- and S-rich or Fe- and O-rich structures were observed. Precipitates of iron sulfides were described for Lihir Island, Papua New Guinea, due to the interaction of hydrothermal gas and liquid, seawater, and Fe-rich sediments (Pichler et al., 1999a). When hydrothermal H_2S is in contact with oxygenated seawater, H_2SO_4 forms, leading to the simultaneous dissolution of primary Fe-rich sediment grains and to the formation of marcasite (FeS_2) and pyrite (FeS_2) (Pichler et al., 1999a). It is possible that a similar mechanism takes place in the formation of Fe and S rich particles found in the sample HF1. In the case of Fe—O rich particles found in the hydrothermal system of Papua New Guinea, the interaction of Fe-rich hydrothermal fluids with seawater appears to be the factor controlling the crystalline formation of Fe(III) oxy-hydroxides during its precipitation at a temperature range between 60 and 93 °C.

Additionally, the role of other parameters, such as interactions with dissolved organic matter (DOM), the presence of adsorbing agents (e.g., Fe particles) or ultra violet radiation in the speciation of metals and metalloids in aqueous systems are complex and proven to play a role in a shallow-water hydrothermal system like Paleochori Bay (Callac et al., 2017; Garcia-Pichel and M Bebout, 1996; Gomez-Saez et al., 2015; Mladenov et al., 2010; Price and Giovannelli, 2017). DOM has proven to be relevant for the mobilization of metals like Cu and Fe in shallow hydrothermal systems (Gomez-Saez et al., 2015; Kleint et al., 2015). Furthermore, DOM has been established as a key factor during HgS nanoparticle generation and dissolution in natural seawater (Manceau et al., 2015; Mazrui et al., 2018; Slowey, 2010). Therefore, its influence upon the colloidal (400–40 nm), and in consequence, the nanoparticulate (200–20 nm) fraction of As might be significant, since it can provide thiol groups (-SH) during nucleation of metal-sulfide complexes, probably facilitating the formation of the As—S NPs and potentially even stabilizing the amorphous phase (Gebauer et al., 2009; Manceau et al., 2015; Mazrui et al., 2018; Slowey, 2010).

Finally, in terms of legal regulations, the WHO, established arsenic concentrations in drinking water as harmful if above 10 μg/L, while the EPA gives maximum concentrations in saltwater systems of 63 and 36 μg/L for acute and chronic exposition, respectively. However, all these considerations have been developed without a size range specification of the arsenic fraction including As NP. In Milos, the As-NP fraction can easily exceed these concentration (HF2; $As_{200–20}$, 1.3 μM or 97.4 μg/L) and without knowledge of its chemical behavior in different biological and environmental contexts, the bioaccumulation of arsenic cannot be assumed as a simple model of arsenic ionic species released from the NP.

5. Conclusions

Amorphous As—S NPs with sphere morphology and diameters around 100 nm are described for the first time in an environmental context, specifically in hydrothermal fluids being released into the coastal Mediterranean Sea. The nanoparticulate fraction (between 200 and 20 nm) represent a significant portion of the total soluble arsenic (below 200 nm) concentration, indicating a possible role in the cycling of As in Paleochori Bay, Milos (Greece). A deeper understanding of As NPs and further analyses about their toxicity is required to improve understanding of As geochemistry in aqueous environments influenced by hydrothermal venting.

Supplementary data to this article can be found online at https://doi.org/10.1016/j.marchem.2019.03.008.

Acknowledgements

This study was supported by Conicyt through a fellowship to VDT (Programa de Capital Humano Avanzado, BECAS-Chile, CONICYT, 72160570 Res. Convenio 7359/2015) and by the Deutsche Forschungsgemeinschaft (DFG, Germany) through the Emmy Noether-Program (grant BU 2606/1-1 to SIB), as wells as DFG grant HE 7594/1-1 (TP). We would like to thank Reshma Kadam and Daniel Carmona Rioja for their support in the Advanced Ceramics laboratories, Petra Witte for performing SEM analyses, and Rebecca Aepfler and Christopher Vogel for their helpful hands during fieldwork. Special thanks go to Athanasios Godelitsas for providing the orpiment standard and for logistical support in Athens, and to Antonios Vichos and the Artemis Deluxe rooms for their generous hospitality on Milos. Grateful thanks furthermore go to Wolfgang Bach for his insightful comments on the manuscript.

References

Aiuppa, A., Avino, R., Brusca, L., Caliro, S., Chiodini, G., D'Alessandro, W., Favara, R., Federico, C., Ginevra, W., Inguaggiato, S., Longo, M., Pecoraino, G., Valenza, M., 2006. Mineral control of arsenic content in thermal waters from volcano-hosted hydrothermal systems: insights from island of Ischia and Phlegrean Fields (Campanian Volcanic Province, Italy). Chem. Geol. 229 (4), 313–330.

Akerman, N., Price, R.E., Pichler, T., Amend, J.P., 2011. Energy sources for chemo-lithotrophs in an arsenic- and iron-rich shallow-sea hydrothermal system. Geobiology 9 (5), 436–445.

An, Y., Nie, F., Wang, Z., Zhang, D., 2011. Preparation and characterization of realgar nanoparticles and their inhibitory effect on rat glioma cells. Int. J. Nanomedicine 6, 3187–3194.

AshaRani, P., Low Kah Mun, G., Hande, M., Valiyaveettil, S., 2009. Cytotoxicity and genotoxicity of silver nanoparticles in human cells. ACS Nano 3 (2), 279–290.

Baláž, P., Fabian, M., Pastorek, M., Cholujová, D., Sedlák, J., 2009. Mechanochemical preparation and anticancer effect of realgar (As4S4) nanoparticle. Mater. Lett. 63 (17), 1542–1544.

Baláž, P., Sedlák, J., Pastorek, M., Cholujová, D., Vignarooban, K., Bhosle, S., Boolchand, P., Fabián, M., Bujňáková, Z., 2011. In-vitro testing of arsenic sulfide nanoparticles for the treatment of multiple myeloma cells. NSTI Nanotech. 3 978-1-4398-7138-6.

Baláž, P., Sedlák, J., Pastorek, M., Cholujová, D., Vignarooban, K., Bhosle, S., Boolchand, P., Bujňáková, Z., Dutková, E., Kartachova, O., Stalder, B., 2012. Arsenic sulphide As_4S_4 nanoparticles: physico-chemical properties and anticancer effects. J. Nano. Res. 18-19, 149–155.

Bao, X.-Y., Soci, C., Susac, D., Bratvold, J., Aplin, D.P.R., Wei, W., Chen, C.-Y., Dayeh, S.A., Kavanagh, K.L., Wang, D., 2008. Heteroepitaxial growth of vertical GaAs nanowires on Si (111) substrates by metal−organic chemical vapor deposition. Nano Lett. 8 (11), 3755–3760.

Bauer, M., Blodau, C., 2009. Arsenic distribution in the dissolved, colloidal and particulate size fraction of experimental solutions rich in dissolved organic matter and ferric iron. Geochim. Cosmochim. Ac. 73 (3), 529–542.

Bayraktarov, E., Price, R., Ferdelman, T., Finster, K., 2013. The pH and pCO_2 dependence of sulfate reduction in shallow-sea hydrothermal CO_2 – venting sediments (Milos Island, Greece). Front. Microbiol. 4 (111). https://doi.org/10.3389/fmicb.2013.00111.

Boyd, P.W., Ellwood, M.J., 2010. The biogeochemical cycle of iron in the ocean. Nat. Geosci. 3, 675–682. https://doi.org/10.1038/ngeo964.

Breuer, C., Pichler, T., 2013. Arsenic in marine hydrothermal fluids. Chem. Geol. 348, 2–14. https://doi.org/10.1016/j.chemgeo.2012.10.044.

Brust, M., Walker, M., Bethell, D., Schiffrin, D.J., Whyman, R., 1994. Synthesis of thiol-derivatised gold nanoparticles in a two-phase liquid-liquid system. J. Chem. Soc. Chem. Commun. (7), 801–802. https://doi.org/10.1039/C39940000801.

Bühring, S.I., Sievert, S.M., 2017. The shallow submarine hot vent system off Milos (Greece) – A natural laboratory to study hydrothermal geomicrobiology. In: Kallmeyer, J. (Ed.), Life at Vents and Seeps (Life in Extreme Environments). 5. De Gruyter, pp. 85–106.

Bujňáková, Z., Baláž, P., Makreski, P., Jovanovski, G., Čaplovičová, M., Čaplovič, Ľ., Shpotyuk, O., Ingram, A., Lee, T.-C., Cheng, J.-J., Sedlák, J., Turianicová, E., Zorkovská, A., 2015. Arsenic sulfide nanoparticles prepared by milling: properties, free-volume characterization, and anti-cancer effects. J. Mater. Sci. 50 (4), 1973–1985. https://doi.org/10.1007/s10853-014-8763-5.

Callac, N., Posth, N.R., Rattray, J.E., Yamoah, K.K.Y., Wiech, A., Ivarsson, M., Hemmingsson, C., Kilias, S.P., Argyraki, A., Broman, C., Skogby, H., Smittenberg, R.H., Fru, E.C., 2017. Modes of carbon fixation in an arsenic and CO_2-rich shallow hydrothermal ecosystem. Sci. Rep. 7 (1), 14708. https://doi.org/10.1038/s41598-017-13910-2.

Caporale, A.G., Punamiya, P., Pigna, M., Violante, A., Sarkar, D., 2013. Effect of particle size of drinking-water treatment residuals on the sorption of arsenic in the presence of competing ions. J. Hazard. Mater. 260, 644–651. https://doi.org/10.1016/j.jhazmat.2013.06.023.

Chen, H.-I., Chang, H.Y., 2004. Homogeneous precipitation of cerium dioxide nanoparticles in alcohol/water mixed solvents. Colloids Surf. A Physicochem. Eng. Asp. 242, 61–69.

Choi, D.Y., Madden, S., Wang, R.P., Rode, A., Krolikowska, M., Luther-Davies, B., 2007. Nano-phase separation of arsenic tri-sulphide (As_2S_3) film and its effect on plasma etching. J. Non-Cryst. Solids 353 (8), 953–955. https://doi.org/10.1016/j.jnoncrysol.2006.12.102.

Couture, R.M., Rose, J., Kumar, N., Mitchell, K., Wallschläger, D., Van Cappellen, P., 2013. Sorption of arsenite, arsenate, and thioarsenates to iron oxides and iron sulfides: a kinetic and spectroscopic investigation. Environ. Sci. Technol. 47 (11), 5652–5659. https://doi.org/10.1021/es3049724.

Dando, P.R., Hughes, J.A., Leahy, Y., Niven, S.J., Taylor, L.J., Smith, C., 1995. Gas venting rates from submarine hydrothermal areas around the island of Milos, Hellenic volcanic arc. Cont. Shelf Res. 15 (8), 913–929.

Dando, P.R., Thomm, M., Arab, H., Brehmer, M., Hooper, L.E., Jochimsen, B., Schlesner, H., Stöhr, R., Miquel, J.C., Fowler, S.W., 1998. Microbiology of shallow hydrothermal sites off Palaeochori Bay, Milos (Hellenic Volcanic Arc). Cah. Biol. Mar. 39 (3–4), 369–372.

Dando, P.R., Aliani, S., Arab, H., Bianchi, C.N., Brehmer, M., Cocito Fowlers, S.W., Gundersen, J., Hooper, L.E., Kölbh, R., Kuevere, J., Linke, P., Makropoulosr, K.C., Meloni, R., Miquel, J.C., Morri, C., Müller, S., Robinson, C., Schlesner, H., Sieverts, S., Störr, R., Stüben, D., Thormm, M., Varnavas, S.P., Ziebis, W., 2000. Hydrothermal studies in the Aegean Sea. Phys. Chem. Earth (B) 25 (1), 1–8.

De Yoreo, J.J., Gilbert, P.U., Sommerdijk, N.A., Penn, R.L., Whitelam, S., Joester, D., Zhang, H., Rimer, J.D., Navrotsky, A., Banfield, J.F., Wallace, A.F., Michel, F.M., Meldrum, F.C., Cölfen, H., Dove, P.M., 2015. Crystallization by particle attachment in synthetic, biogenic, and geologic environments. Science 349 (6247), aaa6760.

Douville, É., Charlou, J.-L., Donval, J.-P., Hureau, D., Appriou, P., 1999. Le comportement de l'arsenic (As) et de l'antimoine (Sb) dans les fluides provenant de différents systèmes hydrothermaux océaniques. C. R. Acad. Sci. II – Earth Planet. Sci. 328 (2), 97–104. https://doi.org/10.1016/S1251-8050(99)80004-4.

Du, Y., Yin, Z., Zhu, J., Huang, X., Wu, X.-J., Zeng, Z., Yang, Q., Zhang, H., 2012. A general method for the large-scale synthesis of uniform ultrathin metal sulphide nanocrystals. Nat. Commun. 3, 1177. https://doi.org/10.1038/ncomms2181.

Duran, N., Marcato, P., De Conti, R., Alves, O., Costa, F., Brocchi, M., 2010. Potential use of silver nanoparticles on pathogenic bacteria, their toxicity and possible mechanisms of action. J. Braz. Chem. Soc. 21 (6), 949–959.

Eary, L.E., 1992. The solubility of amorphous As_2S_3 from 25 to 90°C. Geochim. Cosmochim. Acta 56 (6), 2267–2280. https://doi.org/10.1016/0016-7037(92)90188-O.

El-Sayed, M.A., 2001. Some interesting properties of metals confined in time and nanometer space of different shapes. Acc. Chem. Res. 34 (4), 257–264. https://doi.org/10.1021/ar960016n.

El-Sayed, M.A., 2004. Small is different: shape-, size-, and composition-dependent properties of some colloidal semiconductor nanocrystals. Acc. Chem. Res. 37 (5), 326–333. https://doi.org/10.1021/ar020204f.

Ferreira, M. F., Chiu, W. S., Cheok, H. K., Cheang, F., Sun, W., 1996. Accumulation of nutrients and heavy metals in surface sediments near Macao. 32 (5), 420–425.

Filomeni, G., Rotilio, G., Ciriolo, M.R., 2002. Cell signalling and the glutathione redox system. Biochem. Pharmacol. 64 (5–6), 1057–1064.

Floroiu, R.M., Davis, A.P., Torrents, A., 2004. Kinetics and mechanism of As_2S_3(am) dissolution under N_2. Environ. Sci. Technol. 38 (4), 1031–1037. https://doi.org/10.1021/es034292q.

Fru, E.C., Callac, N., Posth, N.R., Argyraki, A., Ling, Y.C., Ivarsson, M., Broman, C., Kilias, S.P., 2018. Arsenic and high affinity phosphate uptake gene distribution in shallow submarine hydrothermal sediments. Biogeochemistry. 141 (1), 41–62.

Garcia-Pichel, F., M Bebout, B., 1996. Penetration of ultraviolet radiation into shallow water sediments: high exposure for photosynthetic communities. Mar. Ecol. Prog. Ser. 131 (1), 257–262.

Gartman, A., Findlay, A.J., Luther, G.W., 2014. Nanoparticulate pyrite and other nanoparticles are a widespread component of hydrothermal vent black smoker emissions. Chem. Geol. 366, 32–41. https://doi.org/10.1016/j.chemgeo.2013.12.013.

Gebauer, D., Cölfen, H., Verch, A., Antonietti, M., 2009. The multiple roles of additives in $CaCO_3$ crystallization: a quantitative case study. Adv. Mater. 21 (4), 435–439.

Gersten, B., 2005. Solvothermal synthesis of nanoparticles. Chemfiles 5, 11–12.

Giovannelli, D., d'Errico, G., Manini, E., Yakimov, M., Vetriani, C., 2013. Diversity and phylogenetic analyses of bacteria from a shallow-water hydrothermal vent in Milos island (Greece). Front. Microbiol. 4, 184.

Godelitsas, A., Price, R.E., Pichler, T., Amend, J., Gamaletsos, P., Göttlicher, J., 2015. Amorphous as-sulfide precipitates from the shallow-water hydrothermal vents off Milos Island(Greece). Mar. Chem. 177, 687–696. https://doi.org/10.1016/j.marchem.2015.09.004.

Goering, J.J., Menzel, D.W., 1965. The nutrient chemistry of the sea surface. Deep-Sea Res. Oceanogr. Abstr. 12 (6), 839–843. https://doi.org/10.1016/0011-7471(65)90807-7.

Gomez-Saez, G.V., Riedel, T., Niggemann, J., Pichler, T., Dittmar, T., Bühring, S.I., 2015. Interaction between iron and dissolved organic matter in a marine shallow hydrothermal system off Dominica Island (Lesser Antilles). Mar. Chem. 177, 677–686. https://doi.org/10.1016/j.marchem.2015.10.003. Part 4.

Grund, S.C., Hanusch, K., Wolf, H.U., 2008. Arsenic and arsenic compounds. In: Ullmann's Encyclopedia of Industrial Chemistry.

Guo, H., Zhang, B., Zhang, Y., 2011. Control of organic and iron colloids on arsenic partition and transport in high arsenic groundwaters in the Hetao basin, Inner Mongolia. Appl. Geochem. 26 (3), 360–370. https://doi.org/10.1016/j.apgeochem.2010.12.009.

Van Hoang, V., Ganguli, D., 2012. Amorphous nanoparticles—experiments and computer simulations. Phys. Rep. 518 (3), 81–140.

Hughes, M.F., 2002. Arsenic toxicity and potential mechanisms of action. Toxicol. Lett.

133 (1), 1–16. https://doi.org/10.1016/S0378-4274(02)00084-X.
Jiang, S., Lee, J.-H., Kim, M.-G., Myung, N.V., Fredrickson, J.K., Sadowsky, M.J., Hur, H.-G., 2009. Biogenic formation of As-S nanotubes by diverse Shewanella strains. Appl. Environ. Microbiol. 75 (21), 6896–6899.
Jomova, K., Jenisova, Z., Feszterova, M., Baros, S., Liska, J., Hudecova, D., Rhodes, C.J., Valko, M., 2011. Arsenic: toxicity, oxidative stress and human disease. J. Appl. Toxicol. 31 (2), 95–107. https://doi.org/10.1002/jat.1649.
Jun, Y.S., Kim, D., Neil, C.W., 2016. Heterogeneous nucleation and growth of nanoparticles at environmental interfaces. Acc. Chem. Res. 49 (9), 1681–1690.
Kadar, E., Fisher, A., Stolpe, B., Harrison, R.M., Parello, F., Lead, J., 2012. Metallic nanoparticle enrichment at low temperature, shallow CO_2 seeps in southern Italy. Mar. Chem. 140-141, 24–32. https://doi.org/10.1016/j.marchem.2012.07.001.
Kleint, C., Kuzmanovski, S., Powell, Z., Bühring, S.I., Sander, S.G., Koschinsky, A., 2015. Organic cu-complexation at the shallow marine hydrothermal vent fields off the coast of Milos (Greece), Dominica (Lesser Antilles) and the Bay of Plenty (New Zealand). Mar. Chem. 173, 244–252.
Lee, J.-H., Kim, M.-G., Yoo, B., Myung, N.V., Maeng, J., Lee, T., Dohnalkova, A.C., Fredrickson, J.K., Sadowsky, M.J., Hur, H.-G., 2007. Biogenic formation of photoactive arsenic-sulfide nanotubes by *Shewanella* sp. strain HN-41. Proc. Natl. Acad. Sci. U. S. A. 104 (51), 20410–20415. https://doi.org/10.1073/pnas.0707595104.
Lengke, M.F., Tempel, R.N., 2001. Kinetic rates of amorphous As_2S_3 oxidation at 25 to 40°C and initial pH of 7.3 to 9.4. Geochim. Cosmochim. Acta 65 (14), 2241–2255.
Li, X.-S., Xu, L.-D., Zhu, G.-T., Yuan, B.-F., Feng, Y.-Q., 2012. Zirconium arsenate-modified magnetic nanoparticles: preparation, characterization and application to the enrichment of phosphopeptides. Analyst. 137 (4), 959–967. https://doi.org/10.1039/C2AN15985F.
Los, C., Bach, W., 2018. Sulfidation of major rock types of the oceanic lithosphere; An experimental study at 250 °C and 400 bars. Lithos 323, 208–217. https://doi.org/10.1016/j.lithos.2018.02.006.
Malik, M.A., O'Brien, P., Norager, S., Smith, J., 2003. Gallium arsenide nanoparticles: synthesis and characterisation. J. Mater. Chem. 13 (10), 2591–2595. https://doi.org/10.1039/B305860N.
Malik, M.A., O'Brien, P., Helliwell, M., 2005. A new synthesis of InAs quantum dots from $[^tBu_2AsInEt_2]_2$. J. Mater. Chem. 15 (14), 1463–1467. https://doi.org/10.1039/B416944A.
Manceau, A., Lemouchi, C., Enescu, M., Gaillot, A.C., Lanson, M., Magnin, V., Glatzel, P., Poulin, B.A., Ryan, J.N., Aiken, G.R., Gautier-Luneau, I., 2015. Formation of mercury sulfide from Hg (II)–thiolate complexes in natural organic matter. Environ. Sci. Technol. 49 (16), 9787–9796.
Mane, R.S., Sankapal, B.R., Lokhande, C.D., 2000. Thickness dependent properties of chemically deposited As_2S_3 thin films from thioacetamide bath. Mater. Chem. Phys. 64 (3), 215–221. https://doi.org/10.1016/S0254-0584(99)00261-8.
Mane, R.S., Todkar, V.V., Lokhande, C.D., 2004. Low temperature synthesis of nanocrystalline As_2S_3 thin films using novel chemical bath deposition route. Appl. Surf. Sci. 227 (1), 48–55. https://doi.org/10.1016/j.apsusc.2003.10.052.
Masala, O., Seshadri, R., 2004. Synthesis routes for large volumes of nanoparticles. Annu. Rev. Mater. Res. 34, 41–81.
Mazrui, N.M., Seelen, E., King'ondu, C.K., Thota, S., Awino, J., Rouge, J., Zhao, J., Mason, R.P., 2018. The precipitation, growth and stability of mercury sulfide nanoparticles formed in the presence of marine dissolved organic matter. Environ. Sci. Process Imp. 20 (4), 642–656.
Meier, D.V., Pjevac, P., Bach, W., Markert, S., Schweder, T., Jamieson, J., Petersen, S., Amann, R., Meyerdierks, A., *et al* (2019). Microbial metal-sulfide oxidation in inactive hydrothermal vent chimneys suggested by metagenomic and metaproteomic analyses. Environ. Microbiol. 21, 682–701.
Meyer-Dombard, D.R., Price, R.E., Pichler, T., Amend, J.P., 2012. Prokaryotic populations in heated, arsenic-rich sediments of a shallow-sea hydrothermal system, Ambitle Island, Papua New Guinea. Geomicrobiol J. 29, 1–17.
Mladenov, N., Zheng, Y., Miller, M.P., Nemergut, D.R., Legg, T., Simone, B., Hageman, C., Moshiur Rahman, M., Matin Ahmed, K., McKnight, D.M., 2010. Dissolved organic matter sources and consequences for Iron and arsenic mobilization in Bangladesh aquifers. Environ. Sci. Technol. 44 (1), 123–128. https://doi.org/10.1021/es901472g.
Murdock, R., Braydich-Stolle, L., Schrand, A., Schlager, J., Hussain, S., 2008. Characterization of nanomaterial dispersion in solution prior to in vitro exposure using dynamic light scattering technique. Toxicol. Sci. 101 (2), 239–253. https://doi.org/10.1093/toxsci/kfm240.
Neubauer, E., von der Kammer, F., Knorr, K.H., Peiffer, S., Reichert, M., Hofmann, T., 2013. Colloid-associated export of arsenic in stream water during stormflow events. Chem. Geol. 352, 81–91. https://doi.org/10.1016/j.chemgeo.2013.05.017.
Newman, D.K., Beveridge, T.J., Morel, F., 1997. Precipitation of arsenic trisulfide by *Desulfotomaculum auripigmentum*. Appl. Environ. Microbiol. 63 (5), 2022–2028.
Oremland, R.S., Stolz, J.F., 2003. The ecology of arsenic. Science. 300 (5621), 939–944.
Pal, A., Saha, S., Maji, S.K., Kundu, M., Kundu, A., 2012. Wet-chemical synthesis of spherical arsenic nanoparticles by a simple reduction method and its characterization. Adv. Mater. Lett. 3 (3), 177–180.
Pérez-Donoso, J.M., Monrás, J.P., Bravo, D., Aguirre, A., Quest, A.F., Osorio-Román, I.O., Aroca, R.F., Chasteen, T.G., Vásquez, C.C., 2012. Biomimetic, mild chemical synthesis of CdTe-GSH quantum dots with improved biocompatibility. PLoS One 7 (1), e30741. https://doi.org/10.1371/journal.pone.0030741.
Perrière, J., Millon, E., Chamarro, M., Morcrette, M., Andreazza, C., 2001. Formation of GaAs nanocrystals by laser ablation. Appl. Phys. Lett. 78 (19), 2949–2951. https://doi.org/10.1063/1.1370992.
Pichler, T., Mozaffari, A., 2015. Distribution and mobility of geogenic molybdenum and arsenic in a limestone aquifer matrix. Appl. Geochem. 63, 623–633.
Pichler, T., Veizer, J., 1999. Precipitation of Fe(III) oxyhydroxide deposits from shallow-water hydrothermal fluids in Tutum Bay, Ambitle Island, Papua New Guinea. Chem. Geol. 162 (1), 15–31.
Pichler, T., Giggenbach, W.F., McInnnes, B.I.A., Buhl, D., Duck, B., 1999a. Fe sulfide formation due to seawater-gas-sediment interaction in a shallow-water hydrothermal system at Lihir Island, Papua New Guinea. Econ. Geol. 94 (2), 281–288.
Pichler, T., Veizer, J., Hall, G.E., 1999c. Natural input of arsenic into a coral-reef ecosystem by hydrothermal fluids and its removal by Fe (III) oxyhydroxides. Environ. Sci. Technol. 33 (9), 1373–1378.
Pichler, T., Amend, J.P., Garey, J., Hallock, P., Hsia, N.P., Karlen, D.J., Meyer-Dombard, D., McCloskey, B., Price, R.E., 2006. A natural laboratory to study arsenic geobiocomplexity. Eos. 87 (23), 221–225. https://doi.org/10.1029/2006EO230002.
Pichler, T., Biscéré, T., Kinch, J., Zampighi, M., Houlbrèque, F., Rodolfo-Metalpa, R., 2019. Suitability of the shallow water hydrothermal system at Ambitle Island (Papua New Guinea) to study the effect of high pCO_2 on coral reefs. Mar. Pollut. Bull. 138, 148–158.
Prabhu, S., K Poulose, E., 2012. Silver nanoparticles: mechanism of antimicrobial action, synthesis, medical applications, and toxicity effects. Int. Nano Lett. 2 (32).
Price, R.E., Giovannelli, D., 2017. A Review of the Geochemistry and Microbiology of Marine Shallow-Water Hydrothermal Vents. Reference Module in Earth Systems and Environmental Sciencespp. 1–29. https://doi.org/10.1016/B978-0-12-409548-9.09523-3.
Price, R.E., Pichler, T., 2005. Distribution, speciation and bioavailability of arsenic in a shallow-water submarine hydrothermal system, Tutum Bay, Ambitle Island, PNG. Chem. Geol. 224 (1–3), 122–135. https://doi.org/10.1016/j.chemgeo.2005.07.017.
Price, R.E., Amend, J., Pichler, T., 2007. Enhanced geochemical gradients in a marine shallow-water hydrothermal system: unusual arsenic speciation in horizontal and vertical pore water profiles. Appl. Geochem. 22, 2595–2605.
Price, R., Planer-Friedrich, B., Savov, I., Pichler, T., 2010. Arsenic cycling, thioarsenates and orpiment precipitation at a shallow sea hydrothermal system, Milos Island, Greece. In: Jean, J.-S., Bundschuh, J., Bhattacharya, P. (Eds.), Arsenic in Geosphere and Human Diseases: As. 2010. pp. 66–68.
Price, R., London, J., Wallschläger, D., Ruiz-Chancho, M.J., Pichler, T., 2013a. Enhanced bioaccumulation and biotransformation of As in coral reef organisms surrounding a marine shallow-water hydrothermal vent system. Chem. Geol. 348, 48–55.
Price, R.E., Lesniewski, R., Nitzsche, K.S., Meyerdierks, A., Saltikov, C., Pichler, T., Amend, J.P., 2013b. Archaeal and bacterial diversity in an arsenic-rich shallow-sea hydrothermal system undergoing phase separation. Front. Microbiol. 4, 158. https://doi.org/10.3389/fmicb.2013.00158.
Price, R.E., Savov, I., Planer-Friedrich, B., Bühring, S.I., Amend, J., Pichler, T., 2013c. Processes influencing extreme As enrichment in shallow-sea hydrothermal fluids of Milos Island, Greece. Chem. Geol. 348, 15–26. https://doi.org/10.1016/j.chemgeo.2012.06.007.
Rajamathi, M., Seshadri, R., 2003. Oxide and chalcogenide nanoparticles from hydrothermal/Solvothermal reactions. Curr. Opin. Solid State Mater. Sci. 6 (4), 337–345. https://doi.org/10.1016/S1359-0286(02)00029-3.
Rochette, E.A., Bostick, B.C., Li, G., Fendorf, S., 2000. Kinetics of arsenate reduction by dissolved Sulfide. Environ. Sci. Technol. 34 (22), 4714–4720. https://doi.org/10.1021/es000963y.
Rodney, W.S., Malitson, I.H., King, T.A., 1958. Refractive index of arsenic trisulfide. J. Opt. Soc. Am. 48 (9), 633–636. https://doi.org/10.1364/JOSA.48.000633.
Rodríguez-Paéz, J.E., Caballero, A., Villegas, M., Moure, C., Durán, P., Fernández, J., 2001. Controlled precipitation methods: formation mechanism of ZnO nanoparticles. J. Eur. Ceram. Soc. 21 (7), 925–930. https://doi.org/10.1016/S0955-2219(00)00283-1.
Sartale, S.D., Lokhande, C.D., 2000. Preparation and characterization of As_2S_3 thin films deposited using successive ionic layer adsorption and reaction (SILAR) method. Mater. Res. Bull. 35 (8), 1345–1353. https://doi.org/10.1016/S0025-5408(00)00330-5.
Serrano, S., Gomez-Gonzalez, M.A., O'Day, P.A., Laborda, F., Bolea, E., Garrido, F., 2015. Arsenic speciation in the dispersible colloidal fraction of soils from a mine-impacted creek. J. Hazard. Mater. 286, 30–40. https://doi.org/10.1016/j.jhazmat.2014.12.025.
Sharma, V.K., Filip, J., Zboril, R., Varma, R.S., 2015. Natural inorganic nanoparticles - formation, fate, and toxicity in the environment. Chem. Soc. Rev. 44 (23), 8410–8423. https://doi.org/10.1039/C5CS00236B.
Sievert, S.M., Brinkhoff, T., Muyzer, G., Ziebis, V., Kuever, J., 1999. Spatial heterogeneity of bacterial populations along an environmental gradient at a shallow submarine hydrothermal vent near Milos Island (Greece). Appl. Environ. Microbiol. 65 (9), 3834–3842.
Slowey, A.J., 2010. Rate of formation and dissolution of mercury sulfide nanoparticles: the dual role of natural organic matter. Geochim. Cosmochim. Acta 74 (16), 4693–4708.
Smedley, P. L., Kinniburgh, D. G., 2001. Source and Behavior of Arsenic in Natural Waters. United Nations Synthesis Report on Arsenic in Drinking Water. World Health Organization, Geneva, Switzerland. http://www.who.int/water_sanitation_health/dwq/arsenicun1.pdf, p1-61.
Soci, C., Bao, X.-Y., Aplin, D.P.R., Wang, D., 2008. A systematic study on the growth of GaAs nanowires by metal−organic chemical vapor deposition. Nano Lett. 8 (12), 4275–4282. https://doi.org/10.1021/nl801986r.
Sollich, M., Yoshinaga, M.Y., Häusler, S., Price, R.E., Hinrichs, K.-U., Bühring, S.I., 2017. Heat stress dictates microbial lipid composition along a thermal gradient in marine sediments. Front. Microbiol. 8 (1550). https://doi.org/10.3389/fmicb.2017.01550.
Thanh, N.T., Maclean, N., Mahiddine, S., 2014. Mechanisms of nucleation and growth of nanoparticles in solution. Chem. Rev. 114 (15), 7610–7630.
Tichá, H., Tichý, L., Nagels, P., Sleeckx, E., Callaerts, R., 2000. Temperature dependence of the optical gap in thin amorphous films of As_2S_3, As_2Se_3 and other basic non-

crystalline chalcogenides. J. Phys. Chem. Solids 61 (4), 545–550. https://doi.org/10.1016/S0022-3697(99)00249-8.

Ubale, A., Kantale, J.S., Choudhari, D.M., Mitkari, V.N., Nikam, M.S., Belkhedkar, M., 2013. Characterization of nanostructured As_2S_3 thin films synthesized at room temperature by chemical bath deposition method using various complexing agents. Thin Solid Films 542, 160–166. https://doi.org/10.1016/j.tsf.2013.07.011.

Velea, A., Popescu, M., Sava, F., Lőrinczi, A., Simandan, I.D., Socol, G., Mihailescu, I.N., Stefan, N., Jipa, F., Zamfirescu, M., Kiss, A., Braic, V., 2012. Photoexpansion and nano-lenslet formation in amorphous As_2S_3 thin films by 800 nm femtosecond laser irradiation. J. Appl. Phys. 112 (3), 033105. https://doi.org/10.1063/1.4745021.

Wang, J., Lin, M., Zhang, T., Yan, Y., Ho, P.C., Xu, Q.-H., Loh, K.P., 2008. Arsenic(II) Sulfide quantum dots prepared by a wet process from its bulk. J. Am. Chem. Soc. 130 (35), 11596–11597. https://doi.org/10.1021/ja804436w.

Wu, J.-Z., Ho, P.C., 2006. Evaluation of the in vitro activity and in vivo bioavailability of realgar nanoparticles prepared by cryo-grinding. Eur. J. Pharm. Sci. 29 (1), 35–44. https://doi.org/10.1016/j.ejps.2006.05.002.

Wu, J., Feng, Y., Lin, H., Ho, P.C., 2017. Studies on orpiment (As_2S_3) quantum dots and their self-assemblies. Aust. J. Chem. 70 (10), 1093–1098. https://doi.org/10.1071/CH17194.

Xia, T., Kovochich, M., Liong, M., Mädler, L., Gilbert, B., Shi, H., Yeh, J.I., Zink, J.I., Nel, A.E., 2008. Comparison of the mechanism of toxicity of zinc oxide and cerium oxide nanoparticles based on dissolution and oxidative stress properties. ACS Nano 2 (10), 2121–2134. https://doi.org/10.1021/nn800511k.

Yesugade, N.S., Lokhande, C.D., Bhosale, C.H., 1995. Structural and optical properties of electrodeposited Bi_2S_3, Sb_2S_3 and As_2S_3 thin films. Thin Solid Films 263 (2), 145–149. https://doi.org/10.1016/0040-6090(95)06577-6.

Yücel, M., 2013. Down the thermodynamic ladder: a comparative study of marine redox gradients across diverse sedimentary environments. Estuar. Coast. Shelf Sci. 131, 83–92.

Yücel, M., Gartman, A., Chan, C.S., Luther, G.W., 2011. Hydrothermal vents as a kinetically stable source of iron-sulphide-bearing nanoparticles to the ocean. Nat. Geosci. 4 (6), 367–371. http://www.nature.com/ngeo/journal/v4/n6/abs/ngeo1148.html#supplementary-information.

Yücel, M., Sievert, S.M., Vetriani, C., Foustoukos, D.I., Giovannelli, D., Le Bris, N., 2013. Eco-geochemical dynamics of a shallow-water hydrothermal vent system at Milos Island, Aegean Sea (Eastern Mediterranean). Chem. Geol. 356, 11–20. https://doi.org/10.1038/NGEO1148.

Zhang, J., Zhang, D., 2010. Photoluminescence and growth kinetics of high-quality indium arsenide and InAs-based Core/Shell colloidal nanocrystals synthesized using arsine (AsH_3) generated via zinc arsenide as the arsenic source. Chem. Mater. 22 (4), 1579–1584. https://doi.org/10.1021/cm902912e.

Zhao, Q.-H., Zhang, Y., Liu, Y., Wang, H.-L., Shen, Y.-Y., Yang, W.-J., Wen, L.-P., 2009. Anticancer effect of realgar nanoparticles on mouse melanoma skin cancer in vivo via transdermal drug delivery. Med. Oncol. 27 (2), 203–212. https://doi.org/10.1007/s12032-009-9192-1.

Zhao, W., Lu, X., Yuan, Y., Liu, C., Yang, B., Hong, H., Wang, G., Zeng, F., 2011. Effect of size and processing method on the cytotoxicity of realgar nanoparticles in cancer cell lines. Int. J. Nanomedicine 6, 1569–1577.